

Available online at www.sciencedirect.com



ELEGTROCHIMICA Acta

Electrochimica Acta 49 (2003) 3-21

www.elsevier.com/locate/electacta

A model for charge transfer inverse photoemission

Shachi Gosavi, R.A. Marcus*

Arthur Amos Noyes Laboratory of Chemical Physics, MC-127-72, Division of Chemistry and Chemical Engineering, California Institute of Technology, Pasadena, CA 91125, USA

Received 16 June 2003; accepted 17 July 2003

Abstract

Charge transfer inverse photoemission spectroscopy (CTRIPS), the phenomenon of inverse photoemission at a metal–solution interface, has been the subject of a variety of experiments. An approximate theoretical model is presented which includes (1) the electronic structure of the metal; (2) the principal features of the emission spectra, such as the high and low frequency thresholds at a given injection energy of the electron or hole, and the intensity of the light emission versus electrode potential; (3) the role of surface states; and (4) the question of direct versus indirect radiative transitions. A broad array of experiments from different groups is surveyed and treated. There is a considerable need for experiments to fill many missing "gaps" in the data, and various experiments are suggested.

© 2003 Elsevier Ltd. All rights reserved.

Keywords: CTRIPS; Charge transfer inverse photoemission; Electrode photoemission; Pt (111); Au (111); Metal-solution photoemission; Theory

1. Introduction

Inverse photoemission [1–3] at metal–vacuum interfaces has been extensively studied and used to map the empty electronic states in the band structures of metals. Several years ago, McIntyre and Sass [4] performed experiments at a metal-solution interface that were similar in nature to vacuum inverse photoemission spectroscopy (IPS). In their experiments, they used an electron transfer redox agent in solution to inject electrons or holes into a metal electrode and create electronically excited states of the metal. These excited states decayed radiatively and nonradiatively, resulting in a very small quantum yield of the light emission. Because of the electrochemical nature of the experiments, the electrode-solution potential difference could be varied, and the resulting light emission depended on the redox agent-metal potential difference. Although low in intensity, this spectrum was analyzed and provided information on the electronic structure of the metal above and below its Fermi level. The electrochemical experimental technique was termed charge transfer inverse photoemission spectroscopy (CTRIPS). A schematic diagram of phenomenon is given in Fig. 1.

E-mail address: ram@caltech.edu (R.A. Marcus).

The purpose of the present article is twofold. First, a theoretical model is presented for the electron transfer process and the light emission. A possible explanation of the data is given in terms of the model, using tight-binding parameters for the metal, with the experimental band structures obtained from vacuum inverse photoemission and solution electroreflectance (ER) experiments. Second, there is a wide assortment of data, though frequently no two laboratories have used conditions which serve as a check. The available CTRIPS data are assembled and their principal features summarized. In the process some inconsistencies in the data are also noted. Experimental tests of the model are proposed, with the aim of clarifying various features of the spectra.

A simple model for vacuum inverse photoemission extensively used in the solid state physics literature [1] consists of three steps: (1) electron injection into the metal, (2) electron transport within the metal and relaxation of the electron by electron–electron collisions, and (3) emission of light (mostly by direct vertical transitions). In this article, we extend the above treatment so as to include in step (1) electron or hole injection by electron transfer between the metal and a reactant in solution and the role of Franck–Condon factors in this electron transfer. The Franck–Condon factors arise from nuclear motion, e.g. the solvent, and result from the reaction satisfying the Franck–Condon principle [5].

The difference between electron injection in vacuum and electron transfer in solution is that in the former the

^{*} Corresponding author. Tel.: +1-626-395-6566; fax: +1-626-792-8485.

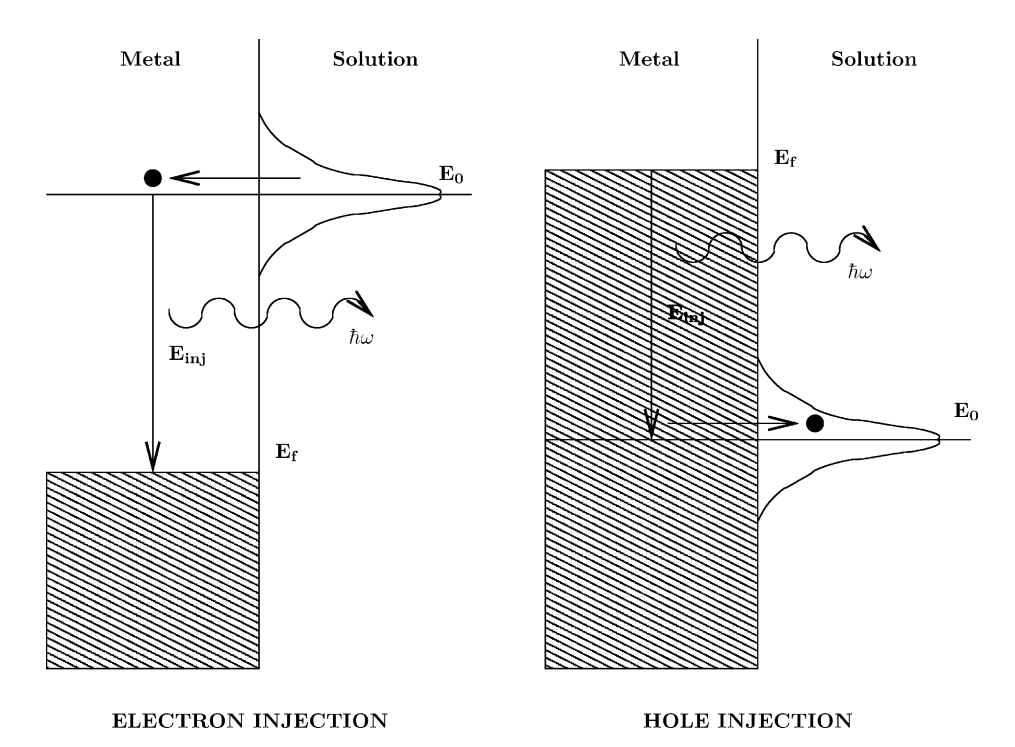


Fig. 1. Schematic diagram for CTRIPS.

electron is injected into a metal energy level 10–100 eV above the vacuum level [1], while in the latter both the energy level entered by the electron and the level to which it then falls lie below the vacuum level and above the Fermi level of the metal. Electronic levels above the vacuum level are free-electron like in nature and in the inverse photoemission experiments their character is assumed to be well known [1]. Thus, the spectrum then provides the properties of the level to which the electron relaxes by photon emission.

In the solution experiments, in contrast, both the initial and the final energy levels are typically bound levels, i.e. below the work function threshold (vacuum level). The optical spectrum emitted in electrochemical inverse photoemission now depends on the detailed band character of both levels. Since the energy difference between the two levels has a maximum of about 3.5 eV in most experiments, due to solution stability constraints, it is not as large as in the vacuum experiments. It is expected from this energy difference that the final band into which the electron relaxes is close to the Fermi level of the metal. Thereby, it is same irrespective of the initial energy level of the electron (hole) unless there is more than one band present at the Fermi level. Accordingly, it is expected that the change in the shape and position of the spectrum on changing the electrode/solution potential will be determined by the presence or absence of radiative bands at the electron injection energy and by the nature of these electronic states.

Electrochemical inverse photoemission spectra have been obtained with different metals, solvents, redox reagents, electrolytes, and electrode-solution potential differences.

The various experiments are summarized in Table 1. The metals affect the spectra through their band structure, while the solvent effect, is at least in part, due to a change in reorganization energy involved in electron transfer. One effect of different redox agents is due to their redox potentials (E_0). The potential of the electrode does not change the positions of the bulk bands relative to the Fermi level (E_F) of the metal electrode. However, it does change their values relative to the energy levels of the redox reagent in solution (E_0), and so strongly affects the emitted spectrum. Although the effect of temperature on photoemission can be substantial, its effect on CTRIPS, has apparently not been studied experimentally.

The role of surface states in CTRIPS has been quite uncertain. In interpreting electroreflectance solution experiments [6], it was inferred that the surface states in a metal are in sufficiently close contact with the solution that a change in the potential of the electrode does not affect them as much as it affects the bulk bands. The metal bulk band energies vary linearly with the electrode potential with a slope of 1, while the surface band energies might be totally pinned to the solution and so not vary at all, depending on the conditions. In this case, the effect of varying the electrode potential in inverse photoemission depends on whether the emitting metal band states are surface states or bulk states. What is actually observed in each experiment should depend on the band structure of the metal and the electrode potential, and this aspect is included in treating the role of the band structure.

The emission spectra have in one instance been sorted into parallel and perpendicular polarization components [7]. They have also been measured in one case at different

Table 1
A summary of the experimental conditions and voltages from various CTRIPS experiments

Authors	Solvent and supporting electrolyte	Donor/acceptor, E_0 vs. reference and vs. SCE (V)	Metal	Reference electrode	Voltage range vs. reference (V)	$E_{\rm inj}$ range (eV)
McIntyre and Sass [4]	MeCN 0.5 M TPABF ₄	Thianthrene: +0.8, 1.18 Benzophenone: -2.0, -1.62	Au(1 1 1)	Ag/AgNO ₃ 10 ⁻³ M	(+0.9, -2.1) (-2.1, +0.9)	(-0.1, 2.9) (-0.1, 2.9)
Ouyang and Bard [11]	MeCN 0.1 M TBABF ₄	Benzophenone: -1.9 , -1.9 t-Stilbene: -2.17 , $-2.17Benzonitrile: -2.22, -2.22$	Pt(111)/polycrystalline Pt	SCE	(+0.2, +1.2) (-0.2, 1.2) (-0.3, +1.2)	(2.1, 3.1) (1.97, 3.37) (1.92, 3.42)
Ouyang and Bard [20]	MeCN 0.1 M TBABF ₄	Thianthrene: +1.1, +1.1 Triphenylamine: +1.1, +1.1 Tris(2,4-dibromophenyl)amine:	Pt	SCE	(+1.6, -1.4)	(-0.5, 2.5) (-0.5, 2.5) (-0.17, 2.83)
		+1.43, +1.43 9,10-Dibromoanthracene: +1.44, +1.44 Benzophenone: -2.0, -2.0	Pt/Rh		(-2.5, +1.0)	(-0.16, 2.84) $(-0.5, 3.0)$
Uosaki et al. [21]	MeCN	Benzophenone: -2.15, -1.71	Au polycrystalline predominantly (1 1 1) faces	$Ag/AgNO_3 10^{-2} M$	(-2.6, +0.7)	(-0.45, 2.85)
	$0.2\mathrm{M}$ TBABF ₄	<i>t</i> -Stilbene: -2.6, -2.16 Benzonitrile: -2.7, -2.26				(0.0, 3.3) (0.1, 3.4)
Murakoshi and Uosaki [22,26]	MeCN	Benzophenone: -2.15 , -1.71	Au and Pt and Pd predominantly (111) faces	$Ag/AgNO_3 10^{-2} M$	(-0.5, +1.1)	(1.65, 3.25)
	0.2 M TBABF ₄	<i>t</i> -Stilbene: -2.6, -2.16 Benzonitrile: -2.7, -2.26				(2.1, 3.7) (2.2, 3.8)
Murakoshi and Uosaki [23]	HMPA	Solvated	Au and Pt predominantly (111) faces	$Ag/AgNO_3 10^{-2} M$	(-1.0, 0.0)	(2.4, 3.4)
	0.2 M NaClO ₄	Electron: -3.4 , -2.96				

A value of $0.38\,\mathrm{V}$ is added to convert from Ag/AgNO₃ ($10^{-3}\,\mathrm{M}$) to SCE, and a value of $0.44\,\mathrm{V}$ is added to convert from Ag/AgNO₃ ($10^{-2}\,\mathrm{M}$) to SCE. In McIntyre and Sass [4], the concentration of TBABF₄ is given as $0.5\,\mathrm{M}$ in the figures but $0.2\,\mathrm{in}$ the text. For light emission due to hole injection $E_{\mathrm{inj}} = E_0 - E_{\mathrm{F}}$.

emission angles [4]. A comprehensive set of experiments of all types is not available for a single system or from a single laboratory, and so some "piecing together" of the diverse data is undertaken in a later section.

The paper is subdivided as follows: in Section 2, a theoretical model is presented for the interpretation of the CTRIPS spectra. A detailed discussion of the experimental results is given in Section 3. Calculations based on the model are given and the results are compared with experiments in Section 4. Consequences of the overall model are given in Section 5. Comparison with an earlier theoretical model is also given in Section 5, and experimental tests of the present mechanism are proposed in Section 6.

2. Theoretical model

2.1. Principal features

The model proposed here for the mechanism of CTRIPS with electron injection can be applied with minor changes to hole injection. We begin with the standard expression [8] for intensity $I(\omega)$ of photon emission between two bands, in terms of $V_{\rm opt}$ the optical coupling between the two bands, and the number of available photon states (proportional to ω^3 [8]) at a given frequency ω :

$$I(\omega) = C\omega^3 |V_{\text{opt}}|^2. \tag{1}$$

Here the numerical constant C contains the dielectric constant ϵ_0 , and the speed of light c [8]. $V_{\rm opt}$ can be calculated using the three-step model.

Step one of the model is the electron injection via an electron transfer to the metal. For simplicity, a nonadiabatic expression (weak interaction) is used, but the main features would apply to the adiabatic case also. The first-order rate constant for a nonadiabatic electron transfer process [5] is given by

$$k_{\rm ET} = \frac{2\pi}{\hbar} FC |H_{\rm DA}|^2, \tag{2}$$

where FC is the expression for the Franck–Condon factor and H_{DA} is the electronic coupling between the donor and the acceptor. This expression is applicable to a redox molecule fixed at some position near the electrode. It is readily modified to the calculation of a second-order electron transfer rate constant [5,9].

The metal electrode has a continum of levels which contribute to the electron transfer process, each level in the metal being represented by a wavevector k. To calculate rate constants at metal surfaces, one needs to model the band structure, and thus the wavevectors of the metal. The three-step model and the next few equations can be used with any model of the metal band structure. In the present paper, we use the tight-binding model for the band structure and for comparison give a treatment using the free-electron model in Appendix A.

For reactions at metal—solution interfaces, the rate constant in Eq. (2) is used to include all the metal—reactant electron transfer energy states, by integrating the right hand side of Eq. (2) over all energies ϵ and all k vectors contributing to a given energy. The energy ϵ is measured relative to the Fermi energy of the metal E_F . Since the Fermi level of the metal E_F is pinned to the potential of the electrode E, the two are used interchangeably in the present article. The rate constant for electron transfer is then given by [5], Eq. (3) when a classical expression (Eq. (4)) is used for the Franck—Condon factor FC.

$$k_{\rm ET} = \frac{2\pi}{\hbar} \int d\epsilon \frac{\mathrm{e}^{-(\lambda - e\eta + \epsilon)^2/4\lambda k_{\rm B}T}}{(4\pi\lambda k_{\rm B}T)^{1/2}} |V(\epsilon)|^2 f(\epsilon), \tag{3}$$

where λ is the "reorganization energy" for the electron transfer, e is the electronic charge, and $e\eta$ is the overpotential, $(E_{\rm F}-E_0)$, E_0 being the standard potential of the redox agent measured on the same scale as $E_{\rm F}$,

$$FC = \frac{e^{-(\lambda - e\eta + \epsilon)^2/4\lambda k_B T}}{(4\pi\lambda k_B T)^{1/2}}.$$
 (4)

The integration over wavevectors in Eq. (3) appears in the square of an averaged coupling matrix element, $|V(\epsilon)|^2$:

$$|V(\epsilon)|^2 = \int d^3 \mathbf{k} |H_{Dk}|^2 \delta(\epsilon(\mathbf{k}) - \epsilon). \tag{5}$$

Here, $|H_{Dk}|$ is the electronic coupling matrix element, $\langle \Psi_D | H | \Psi_k \rangle$, between the donor (D) in solution and the quantum state of the metal represented by the wavevector k. Later, $|V(\epsilon)|^2$ is extended to include the coupling between the upper and lower metal electronic states contributing to the emission of photons. $f(\epsilon)$ in Eq. (3) is the Fermi–Dirac distribution with ϵ measured relative to E_F , the Fermi level of the metal.

$$f(\epsilon) = \frac{e^{\epsilon/k_{\rm B}T}}{1 + e^{\epsilon/k_{\rm B}T}}.$$
 (6)

In the present case, the energy of the donor is much higher (>2 eV) than the Fermi level, and $f(\epsilon)$ is essentially equal to 1. This substitution is made in the following calculations.

Thus far, the effect of the electron transfer process has been included in the expression for photon emission intensity. We also need to consider the details of the metal band structure, i.e. the energetic positions and the nature of the band into which the electron is injected by electron transfer and the band to which the electron relaxes. To obtain the final intensity of photon emission as a function of the overpotential, we need to include the probability that the final state into which the electron relaxes is unoccupied, $f(\epsilon - \eta)$, the Fermi function for a final state. The emitted light intensity is now given by

$$I(\eta,\omega) \propto \omega^{3} \frac{2\pi}{\hbar} \int d\epsilon \frac{e^{-(\lambda - e\eta + \epsilon)^{2}/4\lambda k_{\rm B}T}}{(4\pi\lambda k_{\rm B}T)^{1/2}} |V(\epsilon)|^{2} f(\epsilon - \eta),$$
(7)

where the mean energy level of the metal above the Fermi level into which the electron is injected $E_{\rm inj}$ is the same as the overpotential $e\eta$. The ω is in units of energy (eV). We assume initially, as in the use of the above expression, that any optical absorption by the metal does not alter the shape of the spectrum.

The next step is to derive an expression for $|V(\epsilon)|^2$ using Eq. (5). The inverse photoemission process in the three-step model is, as noted earlier, subdivided into electron transfer (step 1), electron relaxation by a nonradiative process (step 2), and the light emission (step 3). This separation is introduced next into the equation for $|V(\epsilon)|^2$. We begin with an expression very similar to Eq. (5) for pure electron transfer. Upon renaming the initial k by k_1 and ϵ_k by ϵ_1 , and by introducing direct transitions to all states k_2 in the metal, we have

$$|V(\epsilon)|^2 = \iint d^3 \mathbf{k}_2 d^3 \mathbf{k}_1 |H_{Dk_1 k_2}|^2 \delta(\epsilon_1 - \epsilon) \delta(\epsilon_1 - \epsilon_2 - \hbar \omega),$$
(8)

where the second δ function arises from the conservation of energy during the photon emission. $H_{Dk_1k_2}$ includes H_{Dk_1} from Eq. (5) and a term $H_{k_1k_2}$ of the form $\langle \Psi_{k_1}|T|\Psi_{k_2}\rangle$ describing the k_1 to k_2 transition, T being the optical transition coupling operator. Thus,

$$H_{\mathrm{D}k_1k_2} = H_{\mathrm{D}k_1}H_{k_1k_2}.\tag{9}$$

We next introduce a form for the k-wavefunction of metal to calculate the couplings in Eq. (9). In the present article, we use tight-binding wavefunctions. Details of the parameters used in the tight-binding model are given in the next section.

In the present paper, we treat the metal as semi-infinite, occupying the positive side of the z=0 plane. The solution and the donor extend from the z=0 plane into the negative side. The wavefunction of the metal is assumed to go to 0 at z=0, since there are no metal atoms present on the z=0 plane. The distance from the center of the donor to the first lattice plane of the electrode is denoted by z_0 , $z_0 > 0$.

Tight-binding wavefunctions of metals are of the form

$$\Psi_k(\mathbf{r}) = \sum_{j} \sum_{n} u_n \phi_n(\mathbf{r} - \mathbf{R}_j) \exp(i\mathbf{k} \cdot \mathbf{R}_j), \tag{10}$$

where n is an index which ranges over the orbitals, u_n is a coefficient which is calculated from the tight-binding parameters and gives the orbital content of each band, j indexes the periodic sites in the crystal, and $\phi_n(\mathbf{r}-\mathbf{R}_j)$ are the individual wavefunctions of each orbital, n, located at site j. In the present initial exploration of the phenomenon, we assume a simplified form of the orbital wavefunction: $\phi_n(\mathbf{r}-\mathbf{R}_j)$ is assumed to be $\phi_n(\mathbf{R}_j-\mathbf{R}_j)\exp(i\mathbf{k}(\mathbf{r}-\mathbf{R}_j))$ in the Wigner–Seitz cell of the atom and zero everywhere else. This approximation is equivalent to changing the shape of the orbital and replacing it by one whose extent is the Wigner–Seitz cell and whose shape is oscillatory. The actual shape and nature of the orbital are important in the current

calculation only when an overlap between atomic orbitals is required. Such a situation occurs only for the calculation of the overlap of the Gaussian donor with the surface and when the overlap between the two metal bands is required. Since the shape of the Gaussian donor is spherically symmetric, the atomic coupling matrix element will not be affected much by this approximation. For the metal band overlap, the coupling matrix between the two bands is simple, and this approximation is not expected to affect that aspect significantly. While the final wavefunctions with this approximation become free-electron like as in Eq. (11), the calculation needed for obtaining the coefficients is a tight-binding calculation. This approximation reduces the computational complexity, by about a factor of 50, because individual surface atom-donor (Gaussian ball) overlaps do not need to be calculated for each wavefunction. It also facilitates the treatment of the complete planes parallel to the surface instead of a few atoms in each.

Using the approximation described above, Eq. (10) for the tight-binding wavefunctions takes on a modified free-electron form:

$$\Psi_k(\mathbf{r}) = \sum_n u'_n \exp(i\mathbf{k} \cdot \mathbf{r}), \tag{11}$$

i.e. in Eq. (10) $\sum_j \phi_n(\mathbf{r} - \mathbf{R}_j) \exp(i\mathbf{k} \cdot \mathbf{R}_j)$ is approximated by $\exp(i\mathbf{k} \cdot \mathbf{r})$ $\phi_n(0)$ and u'_n equals $u_n\phi_n(0)$. Here, u'_n and \mathbf{k} contributing to a given energy are calculated from the tight-binding parameters. \mathbf{k} can also be written as $\mathbf{k}_{\parallel} + k_{\perp}\mathbf{z}$, where \mathbf{k}_{\parallel} is the component of \mathbf{k} , parallel to the surface and $k_{\perp}\mathbf{z}$ is the component perpendicular to the surface, thus $\Psi_k(\mathbf{r})$ can also be written as $\Psi_{k\parallel,k_{\perp}}(\mathbf{r})$.

For the wavefunction of the redox reagent, we use for simplicity a spherically symmetric donor wave function (as is the case for a solvated electron). A Gaussian form is assumed, $B \exp(-(x^2 + y^2 + (z - z_0)^2)/(2\sigma^2))$, with σ^2 being the mean square radius of the donor's wavefunction. In the case of a more complicated donor, an actual electron transfer matrix element would be calculated [10]. However, we expect that the final shape of the spectrum will not be substantially modified, because of the averaging over the various spatial configurations of the donor with respect to the metal.

The overlap integrals arise from the metal wavefunctions in Eq. (11) coupling to the Gaussian form of the donor.² The coupling can then be evaluated assuming a proportion-

¹ In a previous paper [32], we did not need to make this approximation since the number of wavefunctions needed was very small (60–600). In the present paper joint densities of states of two bands need to be calculated. This calculation requires about 10 000–100 000 wavefunctions and so the approximation was made to expedite the calculation.

² Let the planes of the metal perpendicular to the surface be numbered from 1 to $+\infty$. The solvent exists everywhere else (0 to $-\infty$). The boundary condition that is used in the text assumes that the wave function of the metal in Eq. (11), goes to 0 at z=0. The donor wavefunction in Eq. (12) nevertheless penetrates the $z \ge 0$ planes and so has a nonzero overlap with the metal wave function in Eq. (12).

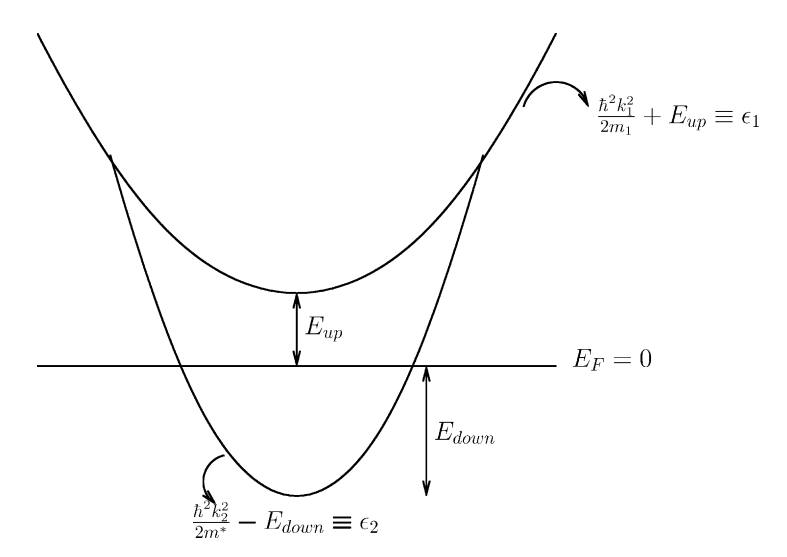


Fig. 2. Two band model for the band structure. m^* and the m_1 are the effective masses of the electrons in the lower and the upper bands, respectively.

ality between the electronic coupling matrix element and the overlap integral,

$$|H_{Dk_1}|^2 = \left| \bar{V} \int_{x, y=-\infty}^{\infty} \int_{z=0}^{\infty} e^{-(x^2 + y^2 + (z - z_0)^2 / 2\sigma^2)} \Psi_{k_1}(\mathbf{r}) \, dx \, dy \, dz \right|^2,$$
(12)

where \bar{V} denotes VB and V is a proportionality constant.

We next consider steps (2) and (3) of the three-step model, namely, relaxation through nonradiative and radiative transitions. The radiative relaxation and resulting photon emission occur due to an allowed coupling, usually transition dipolar in nature, between the initial and final electron states in the metal. This transition dipole coupling depends on the type of bands that exist in the metal. There may also be a direct injection from the electron donor into some surface or bulk states which can give rise to radiationless decay [11]. The surface state coupling is discussed in a later section.

The question of direct versus indirect optical transitions in the photon emission also arises. Direct transitions occur when there exist at least two accessible energy bands, an upper and a lower, at the given k. This type of transition is k-conserving because the emitted photon carries negligible momentum compared to the electron's k. A schematic diagram of such a transition when only two bands are present is given in Fig. 2. In the case of a metal with a surface, only a wavevector conservation of k_{\parallel} , the component of the wavevector parallel to the surface, exists and a vertical transition occurs in this respect between the two accessible energy bands. When the optical transition arises from a wave function that is situated fairly deep in the metal there is also an approximate conservation of the k_{\perp} component. In the present tight-binding treatment, we have not found it necessary to invoke indirect transitions because of the accessibility of the direct transitions in that band structure. However, for the free-electron model, where we fit the vacuum band structure, the upper band is not accessible at some electrode potentials. To account for emission in such cases indirect transitions are included in Appendix A.

In summary, the tight-binding model is used to calculate the contribution to $H_{k_1k_2}$ in Eq. (9) from direct transitions. As mentioned earlier, such transitions conserve $\boldsymbol{k}_{\parallel}$ during the photon emission. Use of the tight-binding wavefunctions yields

$$|H_{k_1k_2}|^2 = \left| \int_{-\infty}^{\infty} \int_{z=0}^{\infty} \Psi_{k_1\parallel,k_{1\perp}}(\boldsymbol{r}) \boldsymbol{T} \Psi_{k_2\parallel,k_{2\perp}}(\boldsymbol{r}) e^{-z/l} d\boldsymbol{r}_{\parallel} dz \right|^2.$$
(13)

The l serves to introduce a phenomenological relaxation of the electron through electron-electron collisions, l being the mean free path of the electron at the energy ϵ [12]. In this form, \mathbf{k}_{\parallel} is taken to be conserved and thus, the broadening is only introduced as an exponential in the z direction [12], $\mathrm{e}^{-z/l}$, and not as an $\mathrm{e}^{-r/l}$. The l decorrelates $k_{1\perp}$ from $k_{2\perp}$ through a Lorentzian broadening serving as a measure of how much the two may differ. T is a matrix which optically couples the orbitals of the two wavefunctions. Here, we assume a simple form where each diagonal element is 0 and each off-diagonal is 1. This form implies zero optical transition dipole moment between two orbitals of the same type, such a coupling being usually forbidden in optical transitions. The integrals over the directions parallel to the surface yield δ functions which give momentum conservation along \mathbf{k}_{\parallel} . The remaining integration is then readily performed.

When no direct transitions can occur then the electrons can radiate only through indirect transitions. Photon emission caused by these transitions has been modeled rigorously [13]. In the present tight-binding calculation, we ignore the contribution of indirect transitions to $H_{k_1k_2}$, but as noted earlier we use indirect transitions in the case of the free-electron model in Appendix A. The details of intensities of direct versus indirect transitions are given there.

Eq. (7) can now be evaluated using a Monte Carlo routine [14] to obtain the light emission intensity.

2.2. Role of surface states

It remains to consider surface states, which in principle can be optically active or inactive. If they are optically active, they can be treated in the same way as bulk states with an extra broadening factor due to an effectively finite length of the states in the z direction. On the other hand, if they facilitate a competitive radiationless transition they then need to be introduced as sinks in the calculation, so reducing the possibility that the electrons radiate.

In the metals considered in this article (Au(111), Pt(111), etc.), no image states but only Shockley surface states have been reported within the energy range of interest above the Fermi level [15]. The Shockley states, intrinsic surface states formed due to the abrupt ending of the metal at z = 0, are of the same electronic character as the band that they arise from. In the present case the band is primarily sp in character. An electron may decay from an sp bulk band to the sp surface band radiatively because of symmetry breaking in the direction of the surface, i.e. the transition dipole matrix element is nonzero only in the z direction. Alternatively, if this breaking of symmetry is not a large perturbation the band character of both bands being sp, this transition may be largely optically forbidden but nonradiatively allowed, and so the electrons may decay nonradiatively through surface states. The optical matrix elements within the metals in the present calculation are assumed to be such that sp-sp transitions are nonradiative. In recent calculations [16] for Pt(111), it was deduced that the d-states were squeezed out of the first layers near the surface. This circumstance might lead to a smaller optical matrix element between bulk d-states and the predominantly sp surface states in the first few layers of the crystal, so causing the surface states to be optically dark for electron injection into Pt(1 1 1).

Next, the position of the surface states with respect to the bulk states needs to be calculated. As inferred from electroreflectance spectroscopy [6,17,18], the position of the surface states depends strongly on the constituents in the solution. The surface states extend beyond the surface of the metal and any specific adsorption of ions on the metal surface leads to a large change in potential at the surface. There have been several models of the electrical double layer at the metal [19] and for some of these models the calculated results [18] have been interpreted as indicating that the energetic position of the surface states can move as much as 1 eV/V with respect to the bulk states on changing electrode potential. This change in energetic position has been attributed to specific adsorption [17,18]. This relative movement implies that while the bulk state potential is changed by changing the electrode potential, the surface states are pinned to the solution potential. In this case, the difference of redox couple potential (E_0) and the surface state potential

($\equiv E_s$) remains approximately independent of changes in the electrode potential. The surface states in the present model are positioned to reflect this behavior and are assumed to be dark states, and so to be states which undergo radiationless decay to the lowest unoccupied states. For simplicity in adjusting their position, they are modeled here using the free-electron model³ and the vacuum band structure given in Fig. 3. Being confined to a few layers near the surface, the surface states have zero real k_z . Thus, they have a dispersion of the form $\hbar^2(k_x^2 + k_y^2)/2m^* - E_{\rm surf}$ (eV). The details of the position of the surface states, i.e. $E_{\rm surf}$ and m^* , are discussed in Section 4.

2.3. Summary of approximations

The phenomenon of CTRIPS has, as discussed above, a number of theoretical features, and the principal simplifying approximations used in the model are summarized as follows:

- 1. A three-step model for the inverse photoemission process: One-step models use the full Hamiltonian and the direct interaction between the donor in the solution and the final energy level in the metal through an optical transition and would be more accurate [1].
- 2. A tight-binding model for the metal band structure, with the use, for calculating H_{Dk_1} in Eq. (9), of simplified orbitals (Eq. (10)) and a Gaussian form for the donor in solution.
- 3. Use of surface state properties measured independently. A linear dependence [17] of surface state energy on metal–solution potential difference was used to locate the position of the surface states. The surface states were modeled using a free-electron model.
- 4. The electron–electron relaxation with the three-step model is introduced through a single mean free path of the form in Eq. (13).
- 5. The variation of the optical matrix elements with energy and band structure, i.e. k, is neglected.

The CTRIP spectrum was calculated using the above approximations and compared with experiments. Before giving the numerical values of the various parameters used and other details of the calculations and the results, we first survey the experimental results.

³ Surface states can also be modelled using the tight-binding parameters and the Z-transform [32]. These states are calculated assuming that the energies of the orbitals of atoms on the surface layer do not get perturbed significantly from their bulk levels. To vary the position of the surface band with respect to the bulk bands these surface energies need to be tuned. We use nine (one s, three p and five d) orbitals in our tight-binding calculations. There are thus nine parameters that can be varied. Instead of tuning these parameter ad hoc, we have chosen to use a free-electron type surface band which uses only one parameter which we determine from experiment.

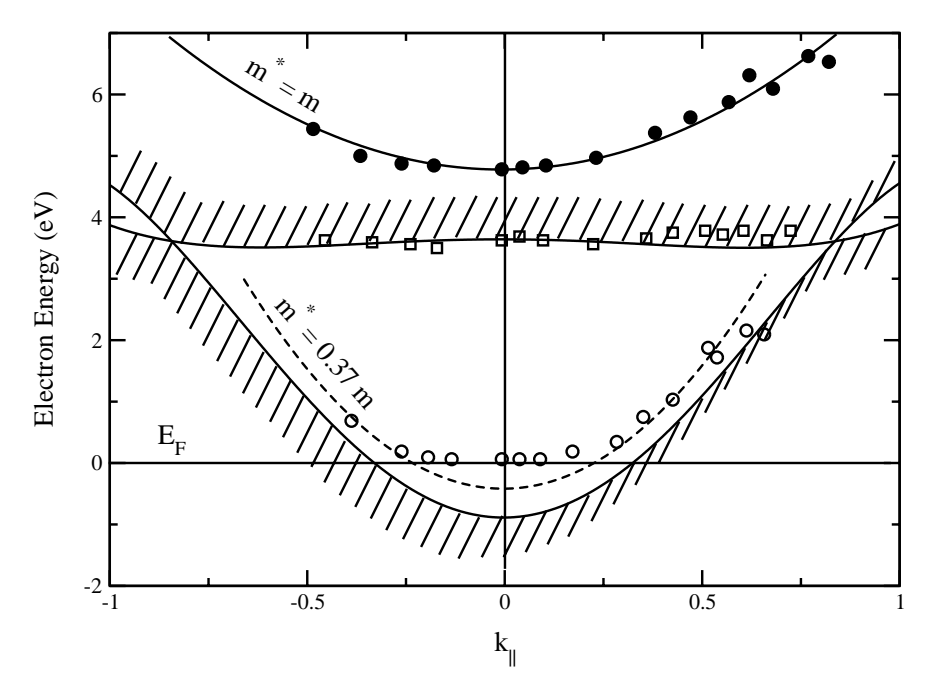


Fig. 3. Measured band structure replotted from [33]. The symbols are experimental measurements. (\bigcirc) denotes the lower band edge while (\square) gives the upper band edge. (\bigcirc) gives the image state. Hatching indicates the projected band structure. The dashed curve is the extrapolation of the dispersion relation obtained below $E_{\rm F}$. m^* is the effective mass of the electron in the given bands.

3. Survey of experimental results

We list below and in Table 1 key experiments from several groups, and include the experimental conditions used. The individual experiments are then discussed and some of the experiments are compared. At present the results exist usually as isolated single-laboratory experiments and have largely not yet been repeated or tested in other laboratories.

- 1. The high energy edge of the emission spectrum varies linearly with potential with unit slope, while the low energy edge is approximately potential-independent [4,7,11,20–23].
- 2. There is a cut-off for the electron injection at Pt surfaces, such that the CTRIPS effect is absent unless the standard potential E_0 of the donor is more negative than $-1.90\,\mathrm{V}$ versus standard calomel electrode (SCE). This effect occurs, regardless of the driving potential, E_F-E_0 [11]. For hole injection at Pt surfaces, there is a cut-off such that the CTRIPS effect again disappears unless E_0 of the acceptor is more positive than $+1.0\,\mathrm{V}$ versus SCE [20]. The question of whether Au also exhibits a cut-off has not been studied.
- 3. The spectra emitted from hole transfer at the Au(111) surface are 50 times more intense in a particular experiment than that from electron transfer [4].
- 4. The spectrum-integrated emission intensity initially increases sharply with electrode potential [11,20,23]. When

- the electrode potential exceeds a certain value, a decrease of intensity has been observed [11,22].⁴
- 5. Molecules having different E_0 's have the same CTRIPS spectral plots, when they have the same driving potential $E_F E_0$, provided the E_0 does not lie outside the cut-off region [20,22].
- 6. For metal films, the emission intensity increases with thickness at low thickness [22].
- 7. Hole emission is strongly polarized in one experiment [7] and also angle-dependent [4].

We consider next in more detail the experimental studies underlying the above findings. In several figures some results have been replotted to make the comparison clearer.

The earliest experiments on CTRIPS are those of McIntyre and Sass [4]. Their experiments were performed primarily using a gold electrode, with acetronitrile as the solvent and benzophenone as the redox reagent. They found that $E_{\rm th}$, the high energy threshold of the spectrum varies linearly with the potential of the electrode E with unit slope. As previously noted, the metal Fermi level is pinned to the electrode potential E. In a later paper [7], they found that $E_{\rm th}$ approximately equals $E_{\rm inj}$, the energy above the Fermi level into which the electron is injected. This result is common to

 $^{^4}$ In [11] the decrease occurs when E > 1.2 V relative to SCE, which translates to E > 0.76 V relative to Ag/Ag⁺ (0.01 M) standard used in [22]. This behavior is roughly consistent with the behavior in Fig. 7 of [22] for benzonitrile and a Pt electrode, where the decrease in emission begins around E > 0.5 V instead of 0.76 V.

the experiments from all groups. E_{inj} equals $(E_{\text{F}} - E_0)$, E_0 being the standard potential of the redox agent measured on the same scale as E_{F} .

They also observed in electron and hole transfer experiments [4a] that the intensity of the hole transfer spectrum is about 50 times greater than that of the electron injection spectrum. They suggested that there were few upper radiative states available for the electron transfer step, due to a band gap at the Au(111) surface above the Fermi level, while the d-states present below the Fermi level of Au(1 1 1) increased the intensity of the hole transfer. They also measured angle-dependent inverse photoemission [4b] and polarization of emission [7a] for Au(111). The detection of polarized light emission provides information about the optical matrix element of the radiative transition. The hole emission showed strongly P-polarized spectra which suggested in this instance sp to d transition. There have been no similar experiments for electron injection. They also compared their emission spectra from gold with that from silver [7b].

Ouyang and Bard presented results [11,20] on the hole and electron transfer spectra at a platinum electrode, again using acetonitrile as the solvent, and presented preliminary results using a rhodium electrode [20a]. In their experiments, they used a series of redox agents with different standard potentials and observed a cut-off in redox potentials below which there was no light emission. This cut-off is denoted below by $E_{\rm R,c}$ for the electron injection and by $E_{\rm O,c}$ for hole injection. They proposed that it arises because of nonradiative Shockley surface states which are present above and below the Fermi level of platinum. They assumed that the surface states decayed in an efficient nonradiative process. On the other hand, if the injection is at an energy where no surface

states are present then a direct radiative transition was free to occur. From their hole and electron transfer experiments, they calculated the band width of the Shockley states in platinum to be about 2.9 eV, which is similar to that obtained independently in solid state experiments [15].

Uosaki and coworkers used a gold electrode and initially used acetonitrile as a solvent [21,22]. Later they used solvated electrons in a hexamethylphosphoramide (HMPA) [23] solvent. In their measurements with the solvated electrons, they again observed an $E_{\rm th} \approx E_{\rm inj}$ as well as a low energy threshold, E_l for the spectra. In the initial study, they concluded that the light emission might involve surface states as acceptor states into which the electrons relax [21a]. Subsequently [22], they compared the position of these surface states with positions of surface states observed in electroreflectance and concluded that surface states do not contribute to the spectrum, since they were already occupied at the potentials used in the CTRIPS experiments.

In another experiment [22], Murakoshi and Uosaki measured the effect of electrode thickness on the intensity of light emission and observed that the spectral intensity increases with increasing electrode thickness [22a], a result attributed to the increase in the number of bulk states with increasing thickness. This fact provided an added basis for their conclusion that bulk states contribute to the emission intensity much more than do surface states. They also compared the spectra from benzonitrile, t-stilbene and benzophenone at the same energy above the Fermi level (E_{inj}) [22b]. Part of their figure is reproduced here in Fig. 4. It is seen that the spectra from benzophenone and benzonitrile overlap very well. Bulk states depend only on the potential of the electrode and thus the bulk band structure depends only

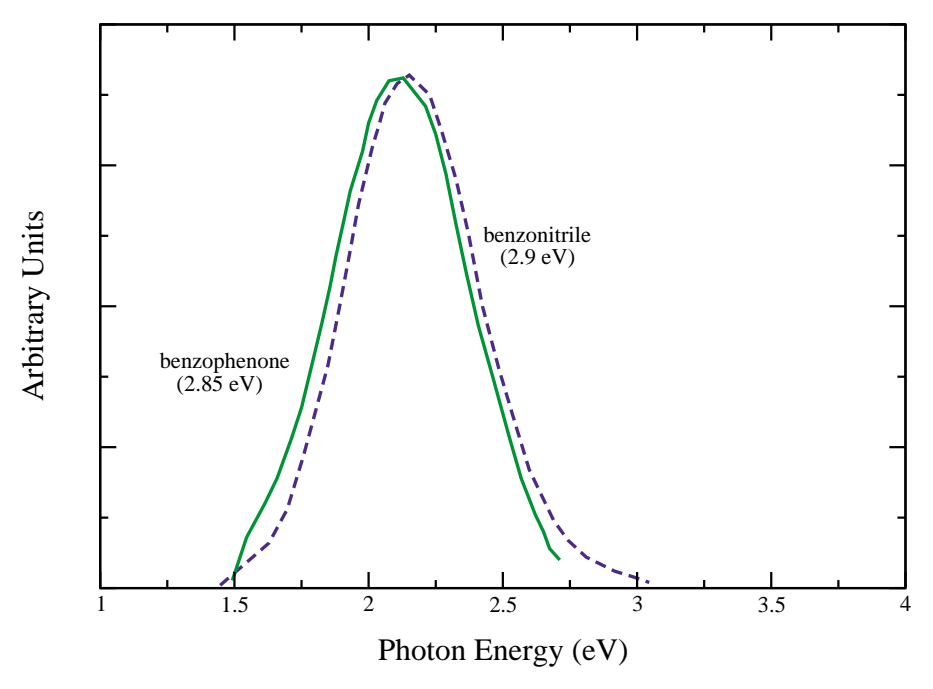


Fig. 4. Inverse photoemission at Au(111) and constant $E_{inj} \approx 2.9 \, \text{eV}$ using different redox agents. Results of Murakoshi and Uosaki [25].

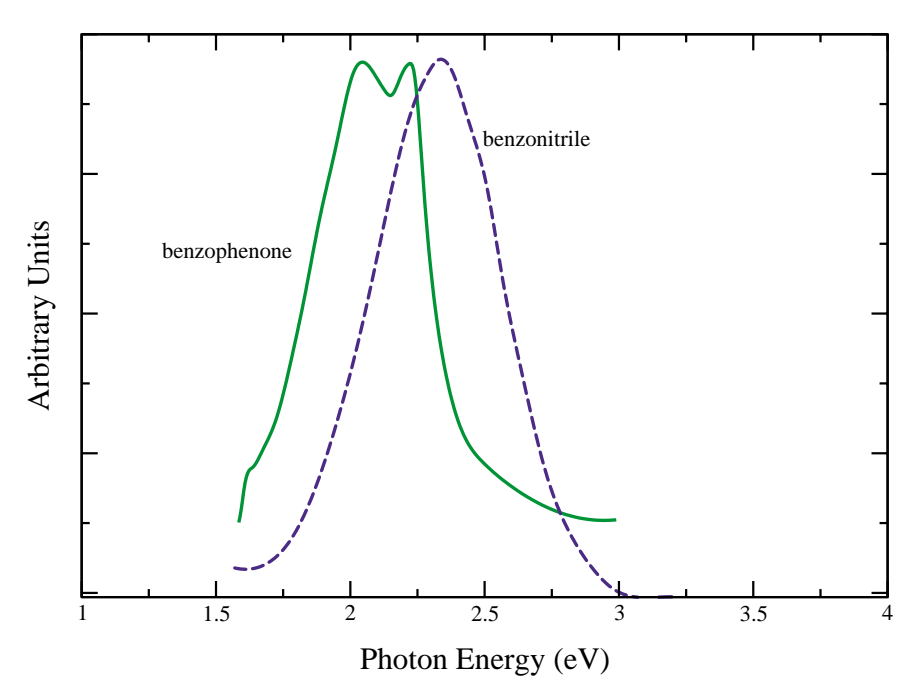


Fig. 5. Inverse photoemission at Au(111) with constant $E_{\rm inj}=2.9\,{\rm eV}$ using different redox agents. (- -) are the results of Murakoshi and Uosaki [25] and (—) are the results of McIntyre and Sass [4].

on $E_{\rm inj}$. From this fact and their data, they concluded that the main contribution to the photon emission is indeed from bulk states.

For comparison we have plotted in Fig. 5, a spectrum from McIntyre and Sass [4c] for benzophenone together with one from Murakoshi and Uosaki [22c] for benzonitrile, both at an $E_{\rm inj}$ of 2.9 eV and for an Au electrode. It is seen

that instead of the spectra coinciding, there is a very large shift, so large that it may reflect some misprint in which one of the measurements may not have been converted to the appropriate relative electrode scale. The one difference in conditions of two experiments is that of the supporting electrolyte, which was tetrapropyl ammonium fluoroborate (TPABF₄) for McIntyre and Sass and tetrabutyl ammonium

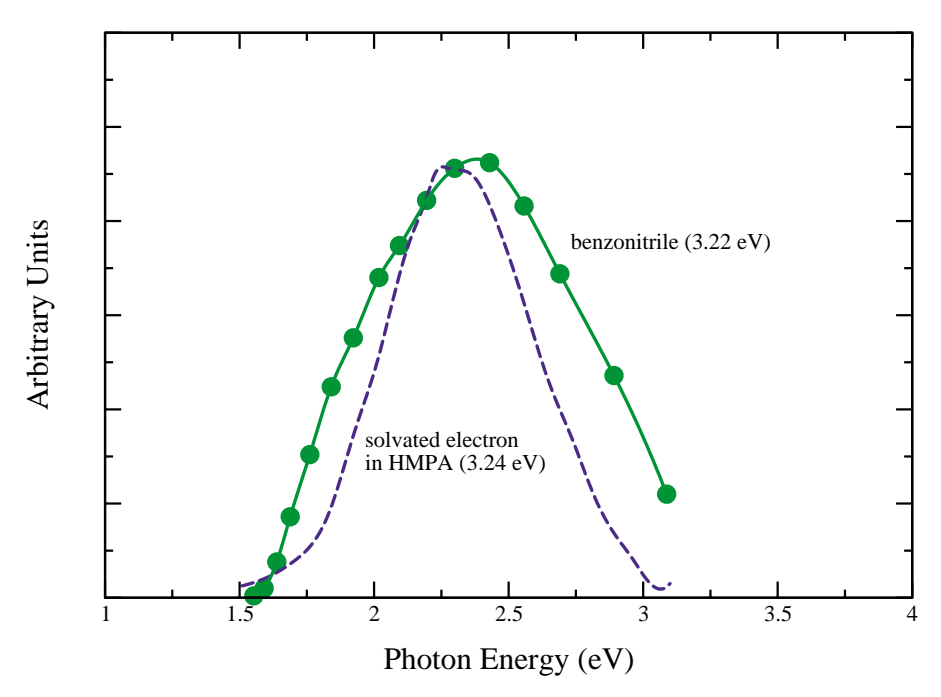


Fig. 6. Inverse photoemission at using different redox agents at the platinum electrode. (- -) are the results of Murakoshi and Uosaki [26] and (-●-) are the results of Ouyang and Bard [11].

fluoroborate (TBABF₄) for Uosaki et al. The effect of the supporting electrolyte and in particular the tetraalkyl ammonium ions [24] is discussed in later sections.

One consequence of the difference in experimental conditions of the various groups may also lie in the difference in the reported E_0 's of the redox couples (Table 1). In the measurement of E_0 values in nonaqueous solvents, there are effects due to liquid junction potentials [24]. To include any differences in E_0 values, we use energy differences in our calculations and comparisons and thus use $E_{\rm inj}$ (i.e. $E_{\rm F}-E_0$) values (Fig. 1) wherever possible. To calculate these $E_{\rm inj}$ values, we use the E_0 measured in the particular experiment. As noted earlier (comment preceding Eq. (3)), $E_{\rm F}$ can be inferred from the electrode potential.

A pair of spectra for platinum are compared in Fig. 6 [11a,22d]. The spectra seem to have the same peak position but are shaped differently. These two studies differ in the solvent used, HMPA in the case of the solvated electron [11] and acetonitrile in the case of benzonitrile, [22]. The spectra of Murakoshi and Uosaki, when plotted versus frequency (e.g. Figs. 4-6, and 9), appear to be more symmetric than the emission spectra of the other two experimental groups. It would be useful in future experiments to establish the exact shape of the spectrum as well as the frequency dependence of the spectra at each energy excess $(E_{\rm F}-E_0)$, by a similar set of studies in a single laboratory. We also note that the plot of spectral emission versus energy in the spectra of Murakoshi and Uosaki is more asymmetric at high injection energies and tends to become symmetric at low injection energies [25,26]. This effect arises from the fact that the low energy threshold is largely unaffected by electrode potential, but the high energy threshold shifts to the red when the driving force $(E_{\rm F}-E_0)$ is reduced.

Uosaki and coworkers plotted the quantum efficiency, Φ , for the benzophenone and benzonitrile systems versus electrode potential [22e]. The curves look remarkably alike when the benzonitrile curve is shifted negatively by the difference in their E_0 's. Thereby, the shape of their spectra appear to depend only on $E_{\rm inj}$ values. They also plotted Φ for the solvated electron at gold and platinum electrodes, [23a] and found that the spectral intensity from platinum is much weaker than that from gold. However, none of the groups have compared the cut-offs from metals ($E_{\rm R,c}$ or $E_{\rm O,c}$) observed by the Bard group for Pt, [11,20] to see if they occur for different metals and if their values depend on the metal.

4. Calculations and results

In the calculations based on the present theory, we consider first the experiments of Murakoshi and Uosaki [23] in which the donor is a solvated electron and the electrode is Au(111). The various properties used to describe the experiment include the tight-binding parameters of Au, the vacuum band structure of Au(111), electroreflectance experiments, and adsorption studies with tetraalkyl ammonium ions.

Tight-binding parameters of gold taken from the literature [27] were used to calculate the wavefunctions of the metal at any given energy. As explained in Section 2, for calculating H_{Dk_1} the individual orbital wavefunctions of each of the atoms of gold are approximated to give a total wavefunction (Eq. (11)) which is free-electron type in form. Gold has a face-centered cubic band structure, and in the experiments the (1 1 1) face was mainly used. We model the same face in our calculation.

We consider next the form and nature of the surface bands. The potential of zero charge (pzc), namely, the electrode potential at which the electrode is uncharged, plays a role in surface properties. When the surface of the electrode is uncharged the double layer at the electrode is quite diffuse. The band structure of the electrode (both bulk and surface bands) at the pzc is then expected to resemble the vacuum band structure of the metal [6,18,19,22], when no specific adsorption is present. The pzc [28] of Au(111) is 0.325 V with respect to the SCE, while that of Pt(111) is 0.85 V [28].

The energy of a surface band changes with respect to that of the bulk bands if the double layer structure at the interface is very dense, an effect which can be caused by the specific adsorption of ions on the surface of the electrode [17]. The cations from most salts (with the exception of the tetraalkyl ammonium salts) are small and highly solvated while the anions are large, with weak solvation shells, and hence are more likely to adsorb. The supporting electrolyte in the case of the solvated electron experiments of Murakoshi and Uosaki is NaClO₄. The ClO₄⁻ ions have been reported to affect the surface states on Au(1 1 1) surfaces [17,18]. We use these data in [17,18] and a free-electron model (see footnote 3) to calculate the surface band. The experimentally measured inverse photoemission vacuum band structure [20] given in Fig. 3 is used to model the surface band at the pzc. Thus, the energy dispersion of the surface band is calculated to be $\hbar^2 (k_r^2 + k_v^2)/2m^* - E_{\text{surf}}$ (eV), where the value of E_{surf} at pzc is taken to be the same as the energy of bottom of the surface band in vacuum (0 for Au(111)). As indicated from [17], E_{surf} varied linearly with $E_{\text{F}} - E_0$ with a slope of $1.0\,\mathrm{eV/V}$ on the positive side and a slope of $0.2\,\mathrm{eV/V}$ on the negatively charged side [17]. The behavior of the positively charged Au(111) [6,18] is attributed [24] to the specific adsorption of the anion. The pzc of Pt(1 1 1), as noted earlier, is 0.85 V versus SCE when the electrolyte is HClO₄. The range of electrode potentials used in these experiments is 0.22–1.44 V versus SCE. The supporting electrolyte in the experiments of Ouyang and Bard [11,20] is tetrabutyl ammonium tetrafluoro borate, TBABF₄. The TBA⁺ ions are known to specifically adsorb on metal surfaces [24,30]. To explain the data of Ouyang and Bard [11,20] and the role of the cut-off, we assume that this adsorption causes a slope of 1.0 eV/V for the change of the surface band energy with respect to the electrode potential on the negative charging side of the electrode. Specific adsorption also changes the pzc and, thus for a clearer interpretation, it is necessary that both the electroreflectance experiments and the CTRIPS

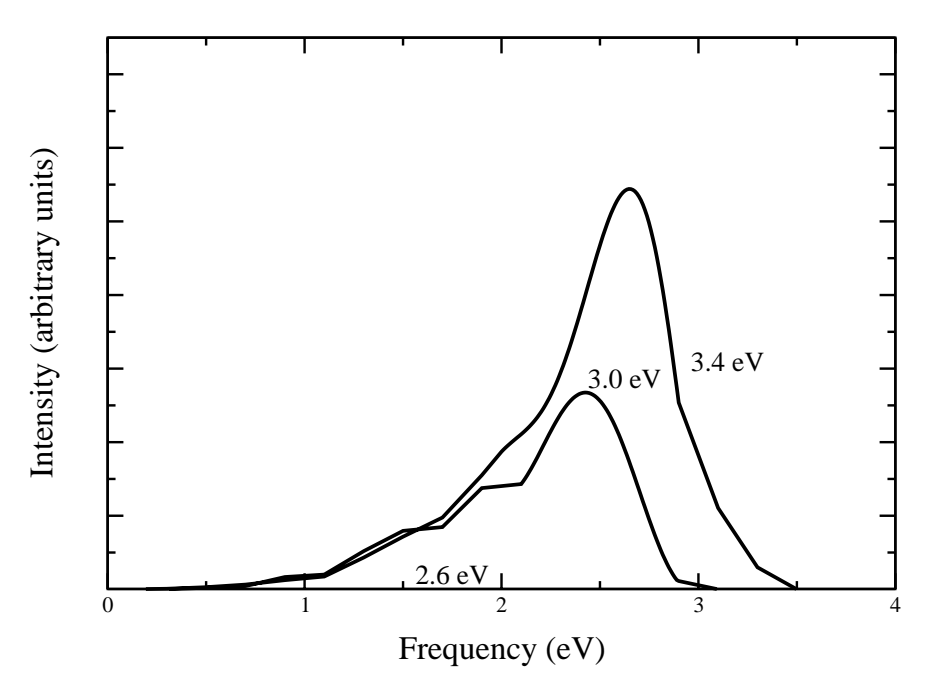


Fig. 7. Light emission intensity from Au with Gaussian orbital as donor. Calculated using the model from Section 2 and tight-binding. The 2.6 eV spectrum cannot be seen on the scale of the other two spectra.

experiments be conducted with the same supporting electrolyte, such as TBABF₄.

In our calculations, we remove an electron from our calculation if it enters a surface band, use a $\lambda=0.4\,\mathrm{eV}$ for the solvated electron [23] and $k_\mathrm{B}T=0.025\,\mathrm{eV}$. The interatomic distance between gold atoms is about 2.88 Å [27] and so, we use a $z_0=3.0$ and $\sigma=1.5\,\mathrm{Å}$. We find that the actual values of and z_0 do not affect results of the calculation very much. An $l=20\,\mathrm{nm}$ [31] is also used.

We also use an adjustable overall normalization factor in the comparison of the calculated integrated emission intensity and the experimental quantum efficiency.

In the CTRIPS experiments of Murakoshi and Uosaki [23] being treated here the electrode potential was varied, leading to an $E_{\rm inj}$ which varied between 2.4 and 3.4 eV. The emission spectrum was measured in each case. The surface band at these voltages [17,22] is low-lying and mostly filled and is expected thereby to have little effect on the spectrum.

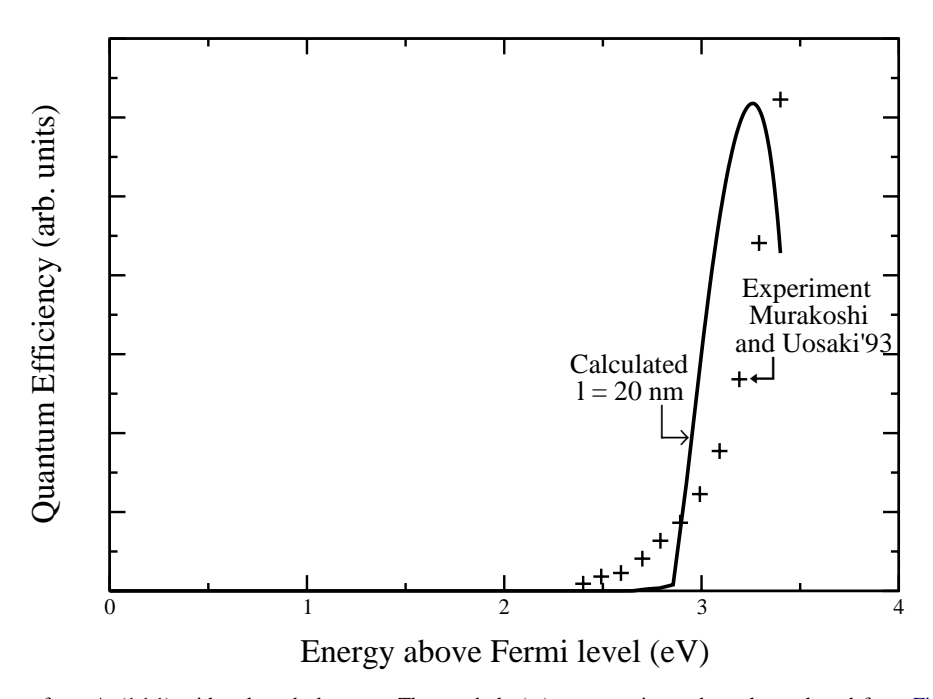


Fig. 8. Quantum efficiency from Au(111) with solvated electrons. The symbols (+) are experimental results replotted from Fig. 5 of [26]. The solid line (-) is calculated using the model from Section 2 and tight-binding with $l=20 \,\mathrm{nm}$.

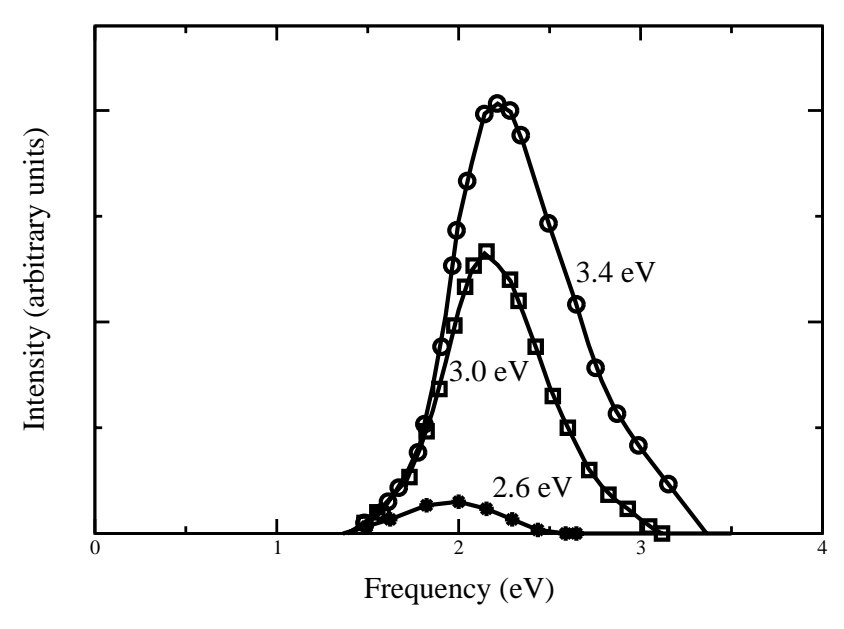


Fig. 9. Emission intensity from Au(111) with solvated electrons. Replotted from Fig. 4 of [26].

In the tight-binding band structure of Au, there are two bands above the Fermi level within this energy range. The edge of the upper band occurs at 2.72 eV relative to the Fermi level, and is also at the edge of the experimental potentials. Also, from Eq. (7), we see that the peak of the spectrum occurs around the experimental driving potential $(E_{\rm inj}) \equiv E_F - E_0$ minus the reorganization energy, i.e. at $(E_F - E_0) - \lambda$. As $E_{\rm inj}$ is lowered from 3.4 to 2.4 eV the upper band contributes less and less (proportional to the tail of a Gaussian) to the emission. The direct transitions are thereby possible in this calculation only via the k_\perp broadening caused by the surface. The Au hole injection spectra of McIntyre and Sass are much more intense than their Au electron injection spectra because the accessible radiative d-states present below the Fermi level give rise to intense direct transitions.

Some results from this model are given in Figs. 7 and 8. We reproduce the corresponding experimental spectra in Figs. 9 and 8. There is moderate agreement between the experimental and the theoretical results. The upper frequency cut-off in the spectra at a given $E_{\rm inj}$ (Fig. 7) arises because the Fermi level serves as the effective cut-off energy for the electron's radiative decay to the lower state.

The decay of the integrated intensity (Fig. 8) at high $E_{\rm inj}$ s occurs because the upper band in the tight-binding model has a relatively flat energy dispersion, and the density of states reduces with energy on going to larger energies.

The l gives the integrated emission intensity curve a shoulder on the low energy side (Fig. 8). The smaller the l the broader the shoulder and the broader the spectrum. We use here a value of l which has been inferred from vacuum—metal interface observations and there is almost no shoulder in our calculations. The actual value of l may be smaller for metal—solution interfaces.

Because of its transparent nature, it is easier to analyze the free-electron model and some calculations using

the free-electron model are given and compared to the tight-binding model in Appendix A.

5. Discussion

We summarize first the consequences of the overall model:

- The electron injected into a bulk state decays radiatively to a bulk state, and yields the emitted spectrum. An electron injected into a surface state decays nonradiatively. Surface states are assumed to be pinned to the solution potential if the supporting electrolyte shows specific adsorption.
- 2. In a bulk state to bulk state radiative decay, a change in film thickness which affects the density of bulk states causes a change in the emitted spectrum, particularly in its intensity [22].
- 3. The $E_{\rm F}$ changes linearly with electrode potential, as do all the bulk state energies. Therefore, the spectrum will not change significantly with change of redox agent (E_0) if the electrode potential is changed in a way so as to compensate for a change of E_0 , i.e. if $E_{\rm F} E_0$ is kept constant.
- 4. In Pt(111), the band structure is such that the cut-off in emission spectra [11,20] can only be explained in the present study by the presence of nonradiative surface states which act as sinks and whose energy does not change with electrode potential, i.e. states whose energy remains constant with respect to the energy of the redox couple. This behavior can only happen if the surface states can sense the potential of the solution more strongly than they sense the potential of the bulk metal. Thus, as assumed in the model, they are pinned to the solution potential while the bulk states move linearly with the electrode potential. Primarily because of the cut-off results of

Ouyang and Bard [11,20], the evidence currently favors surface states which facilitate radiationless transitions.

The principal uncertainty in the present calculation of the position of the upper band is the effect of the solvent. The tight-binding parameters [27] used to calculate the position of the band are fit to reproducing the properties in metal–vacuum experiments, and in these experiments the potential is typically not varied. Further, the profile of the potential drop near the metal surface changes on adding a solution.

The position of the upper band reflects its accessibility and, thereby the shape of the emission spectrum on the high energy side. The less accessible the band, the sharper the calculated fall-off of the spectrum at the high energy side, and the lower the agreement with the observed shape. The accessibility of the band also determines the shape of the integrated intensity of the spectrum and the higher in energy the upper band, the sharper the rise in the integrated intensity of the spectrum.

In some earlier calculations [32], we showed that the wavefunctions that contribute to each band have bulk as well as surface parts. If the surface part of these wavefunctions are pinned to the solution potential, as purely surface states are, then the energetic position of the wavefunctions will be correlated to the solution potential. This correlation might also lead to a shift in the position of band edges. We do not include this effect in the present introductory calculation.

In passing we note, two other mechanisms for radiative transitions that could in principle also give rise to light emission. However, they do not appear to be applicable to the Au, Pt or Pd systems studied:

- 1. In one mechanism, the electron is injected into a surface state and emits radiatively, so reaching a lower unoccupied bulk state. Under specific adsorption [18], the energy of the initial surface state of the electron changes with respect to that of the bulk states as the electrode potential is varied. The relative positions of the surface and bulk states change approximately linearly with potential, with a unit slope, and the spectrum changes accordingly. However, since the surface states on the (111) face of both Pt and Au are low in energy [15], it is unlikely that they contribute to the spectra as injection states.
- 2. In another mechanism, the electron is injected into a bulk state and decays radiatively from the bulk state to a surface state. A change in any property which affects the density of bulk states, such as the electrode thickness, causes a change in the properties of the spectrum, such as intensity. Also, the spectrum changes with potential because of the relative shifts in energies as before. However, this mechanism cannot be used to explain the Pt(111) cut-offs of Ouyang and Bard [11,20] which can be explained by sink states which remain stationary when the electrode potential is changed. In Au(111) on the other hand the surface states are occupied if one assumes specific adsorption. Thus, the surface states are not available for relaxation and light emission.

We note that different types of transitions (surface to bulk, d-bulk to sp-bulk, etc.) might contribute to the CTRIP spectrum at different metal surfaces, and the exact nature and shape of the spectrum depends largely on the band structure of the particular metal and the particular surface symmetry under consideration. Cut-offs of the Bard-type are particularly helpful here, as are the polarization and angle-resolved experiments of McIntyre and Sass.

In concluding this section, we compare our model with that of Murakoshi and Uosaki [23]. Both are three-step models. Three-step models are approximations to the more general on step model [2] of inverse photoemission which describe an overlap between the electron transfer state outside the metal and the final state after photon emission.

In the present article, we employ a model which uses actual expressions for electron transfer into the metal. We assume that the emitted photons arise from k_{\parallel} -conserving direct transitions. In the direction perpendicular to the surface a Lorentzian broadening is introduced to include the effect of the surface. Thus, the intensity of the transitions is determined by how close the $k_{2\perp}$ is to $k_{1\perp}$ and the conservation of k perpendicular to the surface. In the tight-binding model, we ignore the effect of the indirect transitions. The model of Murakoshi and Uosaki [23] is also a three-step model but treats the electron transfer step using a constant energy-independent tunneling probability. The model also assumes no k_{\parallel} -conservation and so no possibility of direct transitions. All the spectral intensity arises from indirect transitions and so the band structure information is introduced into the problem only via the density of states in the metal at a given energy. Thus, any information about band gaps is omitted. Direct transitions and k_{\parallel} -conservation play a major role in inverse photoemission in vacuum at low energies and so are expected to play some role in CTRIPS too. The overall asymmetric shape of the spectra calculated in the present paper nevertheless remains approximately the same as that calculated in [23]. However, using an expression for electron transfer and the band structure of the metal, we find that the low energy cut-off is better described than with an expression which does not contain these details. On the other hand, Murakoshi and Uosaki [23] describe the relaxation processes (step two of the three-step model) more rigorously than the present paper, which introduces electron-electron collisions through a single relaxation length parameter. Also, the present paper neglects any reabsorption⁵ of emitted photons.

⁵ The optical penetration depth of visible photons is about $20 \,\mathrm{nm}$ [23]. This distance is of the same order of magnitude as the vacuum inelastic scattering mean free path, l, that we use. The optical absorption (inverse of the optical penetration depth) can be easily included in our model as an extra relaxation in Eq. (13). If however the l is reduced by the presence of the surface and the solution then the introduction of the optical absorption coefficient might not necessary. In this first calculation, we ignore the effect of the optical absorption coefficient. This reabsorption is treated in [23].

There is a clear need for further experimental results and in the next section we consider possible experiments which may clarify the existing results and provide further insight into CTRIPS and tests of the theoretical model.

6. Proposed experiments

Experiments which may serve to clarify various features of the present mechanism and the CTRIPS phenomena include the following:

- While cut-off experiments were performed for Pt(1 1 1) none have been performed for Au(1 11). The difference in Shockley states in the two metals would yield differences in the cut-offs, if the present mechanism is correct. The position of the Shockley states at the Pt(1 1 1) surface is about 1.2 eV above the Fermi level [15], while those at the Au(1 1 1) surface are slightly above Fermi level [15]. This difference of about 1 eV would be expected to result in a difference in the thresholds for photon emission, if the role of the surface states is nonradiative. From this viewpoint, E_{R,c} for Au(1 1 1) should be about 1 eV lower than that for Pt(1 1 1). An experiment which determines the cut-off E_{R,c} for Au would clearly be useful in clarifying the actual role of the surface states.
- 2. The relative emission intensity of the electron and hole injection has been compared in only a single article [4]. More comparisons of relative intensities of the two emissions in Au(111) are clearly of interest. Au(111) possesses allowed bulk transitions below the Fermi level, while it does not have any allowed bulk transitions above the Fermi level up to about 3.6 eV. On this basis, the hole spectra would be expected to be much more intense than the electron spectra, as was observed in the factor of 50 in the early experiments [4] with Au(111). In Pt(111)the d-states are at the Fermi level and seem not to contribute much to the electron injection spectrum. Assuming that the contribution remains approximately the same in the case of hole emission the hole and electron CTRIP spectra would be similar. It would be useful to have such comparisons for Pt(111), since intensities can give information as to whether a transition is direct or indirect.
- 3. Apart from the initial experiments of McIntyre and Sass there are no experiments on CTRIPS at different angles [4] or with different light polarizations [7]. Angle-resolved spectra for CTRIPS are few and their exact peak structure is not clear. The theoretical model presented in this article uses a tight-binding band structure for the metal. If such experiments become available, the present model can be easily adapted to include accurate coupling matrix elements and to calculate the angle-resolved peak structures in light emission spectra. In the case of vacuum inverse photoemission, *k*-resolved experiments provide detailed information on the positions of band edges and surface states [3]. The con-

tribution to the spectrum in the solution case arises, in contrast with the vacuum experiments, from a wide distribution of k_{\parallel} and k_z , reflected in the fact that in electron transfer the wavefunction of the reactant can be Fourier-decomposed into many such states. Nevertheless, the increasing detail of angle-resolved emission such as that obtained by McIntyre and Sass, can elucidate the energetic positions and angular dispersion of the upper and lower states involved in the emission. To obtain accurate angle-resolved spectra, a more accurate form of the metal wave function using a first principles quantum calculation may ultimately be needed.

Polarization spectra can be interpreted via a model and such experiments can provide information about the optical matrix elements of the transitions and thus about the bands which contribute to the emission. An sp to d transition in the hole study of Au(111) gives P-polarized light [7]. Au(111) has its d band below the Fermi level while Pt(111) has its d band at Fermi level. Comparison of polarization-resolved hole spectra at Pt(111) and Au(111) surfaces could help clarify the role of the d-states in the emission. In some previous calculations [32], we found that d-states contribute much less, per state, than do the sp-states to some electron transfer processes. It is likely that such effects occur in the CTRIPS experiments when the electron or hole is injected into d-states. The reduction in intensity is not expected to occur in the optical matrix element $H_{k_1k_2}$ since the coupling is of a different nature from that in electron transfer H_{Dk_1} .

- 4. Thus far, no effects of concentration or specific adsorption of the supporting electrolyte on the spectrum appear to be available, either in CTRIPS or in electroreflectance experiments. In principle, a decrease in concentration would make the electrical double layer more diffuse and could lead to a smaller effect of electrode potential on the relative position of the surface states with respect to bulk states. A change in the supporting electrolyte from one which specifically adsorbs to one which does not would also lead to a similar change. An example of such an experiment would be one using tetraalkyl ammonium ions with different alkyl chain lengths [24,30]. If there is a significant effect on electroreflectance then there could be a significant effect on CTRIPS.
- 5. We have not explored the possibility that suitable optical experiments may provide added insight into the position of the upper band in the presence of the solvent.

7. Concluding remarks

In the present article, the various experimental results for CTRIPS, are summarized and a theory is proposed for their treatment. This model reproduces approximately the various features of the emission spectra, including the high and low frequency cut-offs at a given $E_{\rm inj}$. The question of the role

of surface states is also addressed. A number of different experiments which serve to test the ideas are proposed. Since the mechanism can depend upon band structure, as discussed in Section 5, such experiments can also help differentiate among possible mechanisms of inverse photoemission. The mechanism proposed in the present paper is applicable to the band structure for Au(1 1 1) and Pt(1 1 1) electrodes. It is expected that different optical transitions will occur at different metal surfaces owing to their diverse band structures. The final spectrum will depend on the type and nature of the energy bands present in the metal surface band structure. Thus, with increasingly detailed experiments it can be expected that CTRIPS can be a useful technique for probing the electronic structure and behavior of metal-solution interfaces. While the once active field of CTRIPS has waned, perhaps reflecting the lack of the experimental-theoretical interaction that has so enriched many other areas of electron transfer chemistry, we hope that the proposed experiments and tests of theoretical ideas may stimulate a revival of this interesting multi-faceted phenomenon.

Acknowledgements

It is a pleasure to acknowledge the support of this research by the Office of Naval Research and the National Science Foundation. This paper was originally intended to be delivered by R.A.M. as the opening lecture of this symposium in honor of the late Prof. Heinz Gerischer. Illness interefered, and this article is dedicated to the memory of this longtime friend.

Appendix A. Free-electron model

Because of the transparent nature of the free-electron model, it is useful to compare its results with those of the tight-binding model. The initial equations for the model are the same as those for the tight-binding model and thus, Eqs. (7)–(9) are still valid. For a free-electron model, however, the metal wavefunction with wavevector k_1 is of the form $A e^{i\mathbf{k}_1 \cdot \mathbf{r}}$ instead of the form given in Eq. (10) or the form given in Eq. (11), which has a modulating factor u'_n at each atom. Since the metal has a surface, this form is changed to one which satisfies boundary conditions at the surface, and the wavefunction becomes modified to [33] A $e^{i(k_{1x}x+k_{1y}y)}$ sin $(k_{1z}z)$, where k_{1z} is the z-component of the wavevector of the metal. Here, the lattice planes are labeled from 1 to ∞ and z is 0 where the zeroth lattice plane would have been present had there been no surface. Using a Gaussian form for the donor, $B \exp(-(x^2 + y^2 + (z - z_0)^{\frac{1}{2}})/(2\sigma^2))$, as before, a coupling matrix element can be calculated:

$$|H_{Dk_1}|^2 = \left| \bar{V} \int_{x,y=-\infty}^{\infty} \int_{z=0}^{\infty} e^{-(x^2 + y^2 + (z - z_0)^2)/2\sigma^2} \right.$$

$$\times e^{i(k_{1x}x + k_{1y}y)} \sin(k_{1z}z) \, dx \, dy \, dz \right|^2. \tag{A.1}$$

The \bar{V} denotes the product VAB, V being the electronic coupling element between the metal atoms and the donor in solution.

In the free-electron model in this appendix, in lieu of a tight-binding parametrization of the band structure, we assume a vacuum-like band structure. In this regime, we also assume that if necessary indirect transitions also contribute to the spectrum. They were not necessary in the tight-binding treatment in this text. When direct transitions are not accessible then the electron can still radiate by indirect transitions. In the relatively crude free-electron model, the upper band is less accessible for injection, and the higher energy edge of the calculated spectrum becomes too steep because only few energies contribute at this edge. Only few energies are accessible, and thus, the edge would take the shape of the Fermi function at that temperature. As explained below, in the present paper the indirect transitions are not assumed to be strong enough to affect the shape of this edge.

For the free-electron model, we first calculate the contribution to $H_{k_1k_2}$ given by Eq. (9) from direct k_{\parallel} -conserving transitions. We use a two-band approximation for the band structure of the metal (Fig. 2) yielding

$$|H_{k_1k_2}|^2 = \left| T \int_{-\infty}^{\infty} \int_{-\infty}^{\infty} \int_{z=0}^{\infty} e^{-i(k_{1x}x + k_{1y}y)} \sin(k_{1z}z) \right|$$

$$\times e^{-i(k_{2x}x + k_{2y}y)} \sin(k_{2z}z) e^{-z/l} dx dy dz \right|^2.$$
(A.2)

As in the tight-binding case, the l, serves to introduce the relaxation of the electron through electron–electron collisions. The integrals over x and y yield δ functions which give momentum conservation along k_{\parallel} . The remaining integral is then easily calculated.

We calculate next the contribution of indirect transitions to $H_{k_1k_2}$. Indirect transitions can also contribute to the photoemission and inverse photoemission processes in vacuum [1,34] and have been modeled rigorously [13]. If no direct transitions can occur then the electrons radiate only through indirect transitions, as noted earlier. In the present free-electron model, indirect transitions are introduced in a simple and quite approximate way.

A broadening term similar to the mean free path broadening but present in all directions is introduced. This term, like the l of the direct transitions decorrelates the k_1 from k_2 . A large broadening allows a calculation of $|H_{k_1k_2}|^2$, by replacing the integral by a constant multiplied by T. This constant which we shall call $T_{\rm ind}$, serves to reduce the entire spectral intensity of the indirect transitions relative to the direct ones. Upon introducing this approximation into the expression for the coupling we have, for $|H_{k_1k_2}|^2$

$$|H_{k_1k_2}|^2 = T_{\text{ind}}^2 T^2. (A.3)$$

Substituting for $H_{k_1k_2}$ and H_{Dk_1} in Eq. (9) and in Eq. (8) we get the $|V(\epsilon)|^2$ for indirect transitions

$$|V(\epsilon)^{2}| = T_{\text{ind}}^{2} T^{2} \iint d^{3} \mathbf{k}_{2} d^{3} \mathbf{k}_{1} |H_{Dk_{1}}|^{2}$$
$$\times \delta(\epsilon_{1}(\mathbf{k}_{1}) - \epsilon) \delta(\epsilon_{1}(\mathbf{k}_{1}) - \hbar\omega - \epsilon_{2}(\mathbf{k}_{2})), \quad (A.4)$$

which is the joint density of states at the two energies ϵ_1 and ϵ_2 , modulated by $|H_{Dk_1}|^2$.

We next consider the band structure of gold within the free-electron model. An experimentally measured (inverse photoemission) vacuum band structure [29] is given in Fig. 3. A particular cross-section of the plot of k_{\parallel} versus energy is shown there (k_{\parallel} has two components k_x and k_y). Three bands exist within the experimentally accessible range: a bulk band at about 3.6 eV above the Fermi level, a surface band which extends above the Fermi level and another bulk band below the surface band. Our free-electron model for the metal is chosen to reproduce these three bands of the metal. Gold has a face-centered cubic band structure, and in the experiments the (1 1 1) face is used. This plane and the fcc structure is used in our tight-binding calculations, but for simplicity, we assume a cubic band structure and a (100) face in our free-electron calculations.

The (100) face is analytically more accessible. With a cubic band structure sine-like wavefunctions can be used for the semi-infinite metal. We use the (111) band structure given in Fig. 3 to model the theoretical (100) band structure. In this way, the surface structure and the band gaps and surface states that are of most interest are described accurately.

As before, the Fermi level of the metal is taken to be the zero of energy. The lower bulk band, ϵ_2 in Fig. 2, is modeled using the form $\hbar^2(k_x^2 + k_y^2 + k_z^2)/2m^* - 7.12$ (eV).

The band gap in our model occurs due to a Brillioum zone cut-off. The upper bulk band is of the form $\hbar^2(k_x^2 + k_y^2 +$ $(k_z^2)/2m_1 + E_{up}$ (eV). The m^* and m_1 are the effective masses of the electron in the lower and the upper bands, respectively, with $m^* = 0.37m$ and $m_1 = 1.0m$, where m is the rest mass of the electron [29]. A plot of the calculated band structure with $E_{\rm up}=3.2\,{\rm eV}$ is given in Fig. 10. We find that an $E_{\rm up} = 3.2 \, \rm eV$ gives the best fit to experimental CTRIPS spectra out of the values of 3.6, 3.4 and 3.2 eV of $E_{\rm up}$. The actual band edge is observed to be located at 3.6 eV at the vacuum-Au(1 1 1) interface [29] instead of 3.2 eV. Band edges are fairly sensitive to the experimental conditions and might shift at the solution-metal interface, but we do not know whether it causes the difference between the two values, or whether the difference reflects the present approximate model used for the indirect transitions. The larger the values of E_{up} used, the sharper the elbow shape of the calculated curve in Fig. 11. We model the surface band as in the case of the tight-binding transitions.

The emission spectrum in [23], was measured at values of $E_{\rm inj}$ between 2.4 and 3.4 eV above the Fermi level of the metal. The upper bulk band in the two-band model occurred at the edge of the experimental voltage. Also, from Eq. (7) we see that the peak of the spectrum will occur around the experimental voltage minus the reorganization energy, i.e. at $(E_{\rm F}-E_0)-\lambda$, as noted earlier. When $E_{\rm inj}$ is lowered from 3.4 to 2.4 eV this band contributes less and less (proportional to the tail of a Gaussian) to the emission. Thus, direct transitions are possible only at the upper end of the experimentally measured potentials. We assume in the calculations a factor of 50 for $T_{\rm ind}$ in Fig. 11, a factor inferred from the results on hole and electron spectra of McIntyre

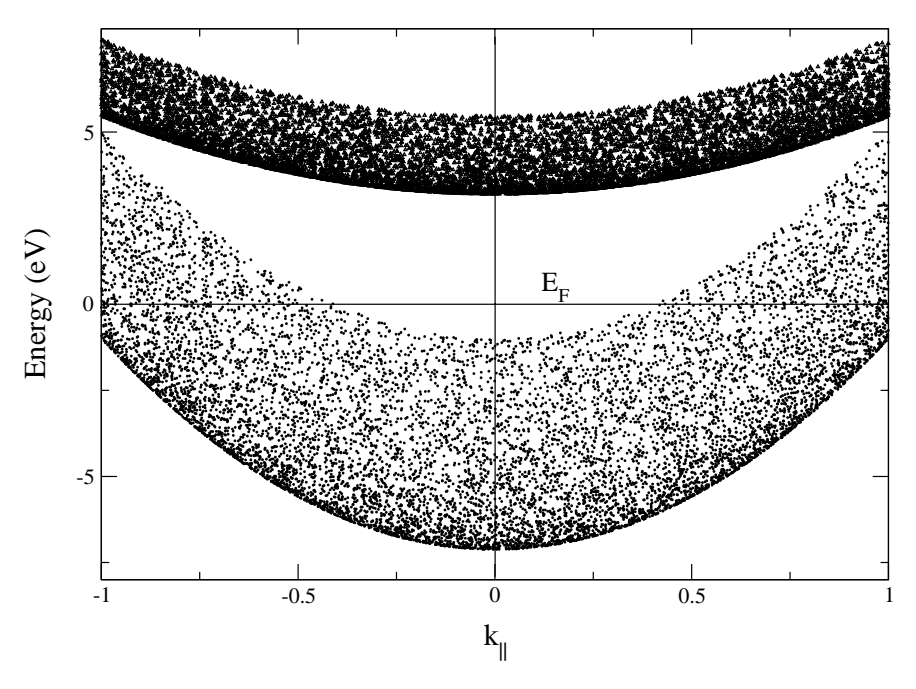


Fig. 10. Projected band structure using the formulae for upper and lower bands given in the text.

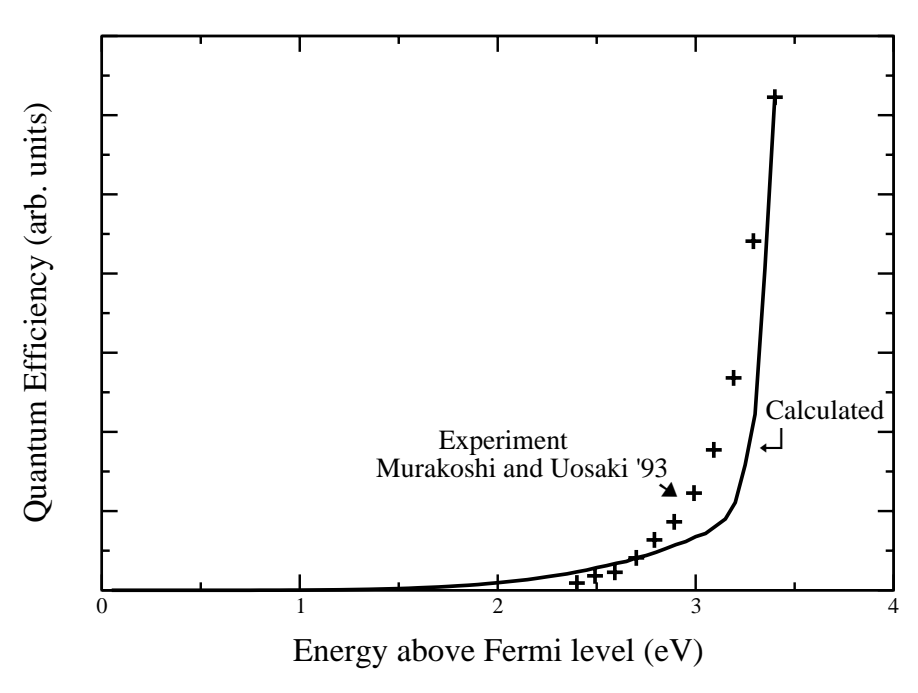


Fig. 11. Quantum efficiency from Au(111) with solvated electrons. The symbols (+) are experimental results replotted from Fig. 5 of [26]. The solid line (—) is calculated using the model from the Appendix A, i.e. the free-electron model.

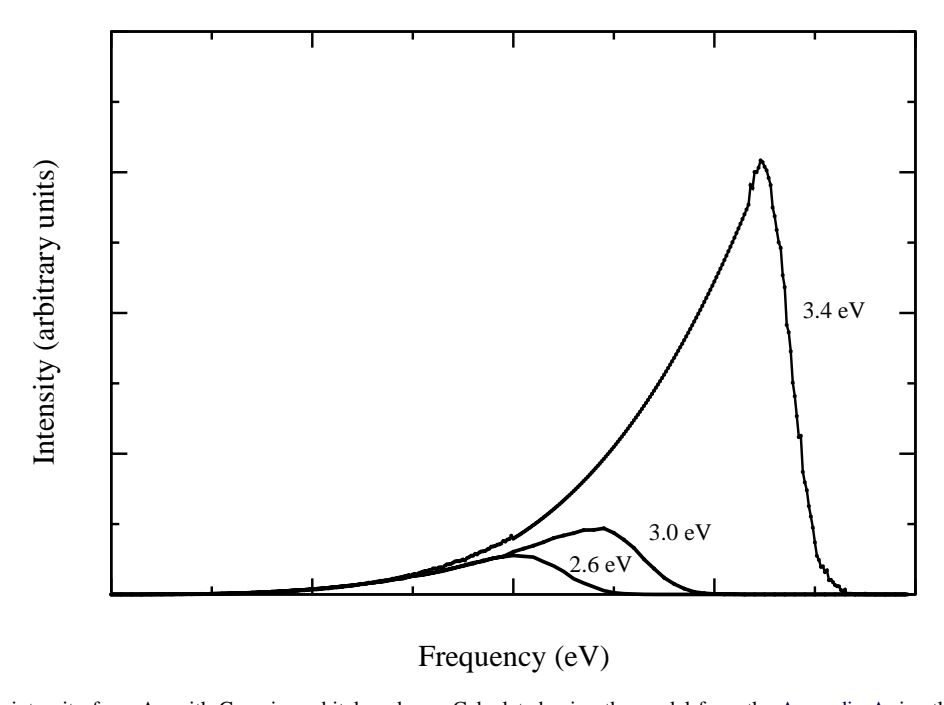


Fig. 12. Light emission intensity from Au with Gaussian orbital as donor. Calculated using the model from the Appendix A, i.e. the free-electron model.

and Sass [4]⁶ as follows: The Au hole injection spectra of McIntyre and Sass are much more intense (by a factor of

 $T_{\rm ind}$) than their Au electron injection spectra because there are no radiative states up to about 3 eV above the Fermi level in gold and they attribute their CTRIP spectra to indirect transitions. The accessible radiative states present below the

 $^{^6}$ The factor $T_{\rm ind}$ is obtained from the difference in light emission intensity between hole and electron transitions at 2.9 eV above and below the Fermi level, respectively. The electron transitions are mainly indirect transitions due to a band gap present above the Fermi level in the $\Gamma-L$ direction of the Au(111) surface [4]. The hole transitions on the other hand are inferred to be direct transitions [4] between a low lying d-band and an sp-band at the Fermi level. The density of d-states is higher than the densities of the sp-bands present above the Fermi level and, this fact

would enter into a more accurate calculation. In an earlier calculation [32], we found that the d-bands couple weakly and thus the contribution from any extra density of states did not make a large difference to the electron transfer rate constant. We use this fact, in the present calculation and, assume that the effective density of states is approximately constant as a function of energy.

Fermi level gives rise to intense direct transitions. We adopt this explanation of McIntyre and Sass for the spectra and use it to calculate T_{ind} .

Results from this model are given in Figs. 11 and 12. We reproduce the corresponding experimental spectra in Figs. 9 and 11. It is easier to analyze the spectra from the free-electron model.

We note that the treatment of indirect transitions in this model is only a first approximation, as reflected in the sharp transition from the direct to indirect transitions shown in the curves obtained from the free-electron model. The lower spectral frequency cut-off arises from the approximate [33] $\sin(k_{1z}z)$ dependence of the matrix element and the shape of the band structure. The lower frequency cut-off occurs at a much higher energy ($\approx 1.5 \,\mathrm{eV}$) in the calculation of direct transitions alone. The addition of indirect transitions lowers it. The upper frequency cut-off arises because the Fermi level serves as the effective cut-off energy for the electron's radiative decay to the lower state. Light emission spectra calculated using the model presented here become more symmetric and show a peak shift to lower energies with an increase in lambda values.

References

- (a) R. Schneider, V. Dose, in: J.C. Fuggle, J.E. Inglesfield (Eds.), Unoccupied Electronic States, Springer-Verlag, 1991;
 - (b) S. Hufner, Photoelectron Spectroscopy, Springer-Verlag, 1996.
- [2] (a) J.B. Pendry, Phys. Rev. Lett. 45 (1980) 16;
 - (b) J.B. Pendry, J. Phys. C 14 (1981) 1381;
 - (c) G. Borstel, G. Thorner, Surf. Sci. Rep. 8 (1987) 1, and references cited therein.
- [3] V. Dose, Surf. Sci. Rep. 5 (1985) 337, and references cited therein.
- [4] R. McIntyre, J.K. Sass, P. R. L. 56 (1986) 651 ((a) Fig. 2 and Fig. 3a, (b) Fig. 3b, (c) Fig. 2: 0.9 V spectrum).
- [5] R.A. Marcus, J. Chem. Phys. 43 (1965) 679, and references cited therein
- [6] S.H. Liu, C. Hinnen, C. Nguyen Van Huong, N.R. De Tacconi, K.M. Ho, J. Electroanal. Chem. 176 (1984) 325.

- [7] R. McIntyre, D.K. Roe, J.K. Sass, H. Gerischer, in: M.P. Soriaga (Ed.), Electrochemical Surface Science, American Chemical Society, Washington, DC, 1988, p. 233 ((a) Fig. 5, (b) Fig. 3), Some early CTRIPS experiments by these authors on several metal and graphite electrodes can be found in the references cited in this article.
- [8] E. Merzbacher, Quantum Mechanics, John Wiley & Sons, 1961, p. 475.
- [9] R.A. Marcus, Electrochim. Acta 13 (1968) 995.
- [10] Y.Q. Gao, R.A. Marcus, J. Chem. Phys. 113 (2000) 6351.
- [11] J. Ouyang, A.J. Bard, J. Phys. Chem. 91 (1987) 4058 ((a) Fig. 7c).
- [12] (a) P.J. Feibelman, D.E. Eastman, Phys. Rev. B 10 (1974) 4932;
 (b) M. Cardona, L. Ley (Eds.), Photoemission in Solids I, Springer-Verlag, 1978, p. 92, references cited therein.
- [13] (a) N.J. Shevchik, Phys. Rev. B 16 (1977) 6428;(b) V.M. Tapilin, Surf. Sci. 383 (1997) 226.
- [14] D. Chandler, Statistical Mechanics, Oxford University Press, 1987.
- [15] C.G. Larsson, P.O. Nilsson, Phys. Lett. A 85A (1981) 393.
- [16] A. Kokalj, M. Causa, J. Phys. Cond. Matter 11 (1999) 7463.
- [17] D.M. Kolb, C. Franke, Appl. Phys. Lett. A 49 (1989) 379.
- [18] D.M. Kolb, Angew Chem. Int. Ed. 40 (2001) 1162, and references cited therein.
- [19] W. Schmickler, Chem. Rev. 96 (1996) 3177, and references cited therein.
- [20] J. Ouyang, A.J. Bard, J. Phys. Chem. 92 (1988) 5201 ((a) Fig. 6).
- [21] K. Uosaki, K. Murakoshi, H. Kita, J. Phys. Chem. 95 (1991) 779 ((a) Fig. 6).
- [22] K. Murakoshi, K. Uosaki, J. Phys. Chem. 96 (1992) 4593 ((a) Fig. 10, (b) Fig. 4, (c) Fig. 2: 0.2 V spectrum, (d) Fig. 4b, (e) Fig. 8).
- [23] K. Murakoshi, K. Uosaki, Phys. Rev. B 47 (1993) 2278 ((a) Fig. 5).
- [24] A.J. Bard, L.R. Faulkner, Electrochemical Methods, John Wiley & Sons, 1980.
- [25] K. Murakoshi, K. Uosaki, J. Electroanal. Chem. 308 (1991) 351.
- [26] K. Murakoshi, K. Uosaki, J. Vac. Sci. Tech. A 10 (1992) 2981.
- [27] D. Papaconstantopoulos, Handbook of Band Structure of Solids, Plenum Press, New York, 1986.
- [28] U.W. Hamm, D. Kramer, R.S. Zhai, D.M. Kolb, J. Electroanal. Chem. 414 (1996) 85.
- [29] D.P. Woodruff, W.A. Royer, N.V. Smith, Phys. Rev. B 34 (1986) 764.
- [30] A.P. Abbott, J.C. Harper, G. Stimsom, J. Electroanal. Chem. 520 (2002) 6. and references cited therein.
- [31] M.P. Seah, W.A. Dench, Surf. Interface Anal. 1 (1979) 2.
- [32] S. Gosavi, R.A. Marcus, J. Phys. Chem. B 104 (2000) 2067.
- [33] Y.Q. Gao, Y. Georgievskii, R.A. Marcus, J. Chem. Phys. 112 (2000) 3358.
- [34] M. Cardona, L. Ley (Eds.), Photoemission in Solids I and II, Springer-Verlag, 1978.